NASA TECHNICAL NOTE

AN IMPROVED METHOD FOR CALCULATING SUPERSONIC PRESSURE FIELDS ABOUT BODIES OF REVOLUTION

by Robert J. Mack

Langley Research Center
Hampton, Va. 23365

NATIONAL AERONAUTICS AND SPACE ADMINISTRATION • WASHINGTON, D. C. • OCTOBER 1971

1. Report No.	2. Government Accession No.	3. Recipient's Catalog No.
NASA TN D-6508		

4. Title and Subtitle

AN IMPROVED METHOD FOR CALCULATING SUPERSONIC PRESSURE FIELDS ABOUT BODIES OF REVOLUTION

5. Report Date: October 1971

6. Performing Organization Code

7. Author(s)

Robert J. Mack

8. Performing Organization Report No.: L-7873

9. Performing Organization Name and Address

NASA Langley Research Center
Hampton, Va. 23365

10. Work Unit No.: 136-13-02-01

11. Contract or Grant No.

12. Sponsoring Agency Name and Address

National Aeronautics and Space Administration
Washington, D.C. 20546

13. Type of Report and Period Covered: Technical Note

14. Sponsoring Agency Code

15. Supplementary Notes

16. Abstract

An improved near-field method for determining supersonic-flow-field properties about a body of revolution is presented and discussed. Comparisons between the improved method, Whitham's theory, and wind-tunnel results are shown for four bodies of revolution – three closed-nose bodies and one ducted body. At Mach numbers of 2.96, 3.83, and 4.63 and ratios of radial distance to body length of 1.0, 2.0, and 5.0, results show that the improved method does reasonably well in predicting flow-field pressure signatures and represents a definite improvement over existing near-field theory. It is also shown that the simple "area balancing" shock prediction technique works reasonably well for bodies with pointed nose sections provided the improved method is used to locate the body flow-field disturbances more exactly.

17. Key Words (Suggested by Author(s))

Supersonic flow field
Bodies of revolution
Sonic boom

18. Distribution Statement

Unclassified – Unlimited

19. Security Classif. (of this report)	20. Security Classif. (of this page)	21. No. of Pages	22. Price*
Unclassified	Unclassified	34	$3.00

*For sale by the National Technical Information Service, Springfield, Virginia 22151

AN IMPROVED METHOD FOR CALCULATING SUPERSONIC PRESSURE FIELDS ABOUT BODIES OF REVOLUTION

By Robert J. Mack
Langley Research Center

SUMMARY

An improved near-field method for determining supersonic-flow-field properties about a body of revolution is presented and discussed. Comparisons between the improved method, Whitham's theory, and wind-tunnel results are shown for four bodies of revolution – three closed-nose bodies and one ducted body. At Mach numbers of 2.96, 3.83, and 4.63 and ratios of radial distance to body length of 1.0, 2.0, and 5.0, results show that the improved method does reasonably well in predicting flow-field pressure signatures and represents a definite improvement over existing near-field theory. It is also shown that the simple "area balancing" shock prediction technique works reasonably well for bodies with pointed nose sections provided the improved method is used to locate the body flow-field disturbances more exactly.

INTRODUCTION

Supersonic-flow-field prediction techniques based on the modified linearized theory of G. B. Whitham (ref. 1) have proved to be successful in the low supersonic to Mach 2.0 speed range. Reference 2 demonstrates this capability for a variety of bodies of revolution and reference 3 shows it extended to aircraft and wing-body combinations.

Recently, wind-tunnel tests were conducted to explore the applicability of existing theory in the high supersonic, low hypersonic speed range (ref. 4). Near-field theory pressure signatures compared well with the measured pressure signatures in the wind-tunnel tests at a Mach number of 2.96. However, disparities between the theoretical signatures and the wind-tunnel measured signatures appeared in the tests at Mach 3.83 and became more pronounced in the tests at Mach 4.63, especially for the low-fineness-ratio bodies and the blunt-nosed bodies. The lack of agreement occurred in nose-shock location, signature shape (particularly pressure gradients), and integrated area under the compression part of the pressure signature.

In this report, corrections to the near-field Whitham solution are presented. Comparisons of wind-tunnel data, near-field theory, and the improved near-field method are also shown. Although these linearized theory solutions are strictly applicable to pointed

bodies ($A'(0) = 0$) or slender ducted bodies ($R(0) \neq 0$ and $R'(0)$ small enough to generate linearized theory disturbances), a method is outlined for use on blunt-nosed bodies $\left(A'(0) \to \infty \text{ or } R'(0) \geq \frac{1}{\beta}\right)$.

SYMBOLS

A	body cross-sectional area
C_p	pressure coefficient
$f(t)$	source distribution function
$F(y)$	Whitham's F function (ref. 1)
$\bar{\bar{F}}(y)$	impulse function defined by equation (8)
h	area influence function (called $h(x)$ in ref. 1)
$k = \frac{(\gamma + 1)M^4}{\sqrt{2\beta^3}}$	
$\bar{k} = \frac{M^2}{\sqrt{2\beta}}$	
l	reference body length
l_n	ducted-nacelle length
$L(y)$	initial source strength function defined by equation (9)
M	Mach number
p	free-stream static pressure
Δp	incremental pressure due to flow field of model
Δp_{max}	maximum value of Δp

r radial distance from body axis

R body radius

R_i body radius at initial Mach plane intersection (see fig. 3(a))

R_f body radius at final Mach plane intersection (see fig. 3(a))

R_{max} maximum body radius

R_β radius where Mach cone is tangent to body

t dummy variable of integration in x-direction

x distance in longitudinal or windward direction, measured from model nose

x_β distance x to where Mach cone is tangent to body (see fig. 3)

x_o distance x to tangent Mach cone apex (see fig. 3)

$x_t = -\beta R_\beta$ (see fig. 3)

y value of characteristic defined in x-direction on body by $y = x - \beta R(x)$, and in flow field by equations (1) and (7)

y_o value of y for which $\int F(y)\,dy$ is maximum

y_1, y_2 values of y which uniquely satisfy the trailing-shock equations

$\beta = \sqrt{M^2 - 1}$

γ ratio of specific heats (1.4 for air)

μ Mach angle

A prime is used to indicate a first derivative. The symbol Δ denotes incremental quantities.

THEORY

From reference 1, the equation of the characteristic (i.e., the loci of points influenced by a given source distribution) can be written as

$$y = x - \beta r + \frac{(\gamma + 1)M^4}{2\beta^2} \int_0^y \left[\frac{\sqrt{y - t + 2\beta r} - \sqrt{y - t + 2\beta R(y)}}{\sqrt{y - t}} \right] f'(t)\, dt$$

$$+ 2M^2 \int_0^y \ln \left\{ \left[\frac{\sqrt{y - t + 2\beta r} - \sqrt{y - t}}{\sqrt{y - t + 2\beta r} + \sqrt{y - t}} \right] \left[\frac{\sqrt{y - t + 2\beta R(y)} + \sqrt{y - t}}{\sqrt{y - t + 2\beta R(y)} - \sqrt{y - t}} \right] \right\} f'(t)\, dt \qquad (1)$$

Using the assumption that $\beta r/y$ is large, equation (1) reduces to

$$y = x - \beta r + kF(y)\sqrt{r} \qquad (2)$$

where

$$F(y) = \int_0^y \frac{f'(t)\, dt}{\sqrt{y - t}} \qquad (3)$$

In this paper, the Stieltjes integral form

$$F(y) = \int_0^y \left[\frac{2}{\beta R(t)} \right]^{1/2} h\left(\frac{y - t}{\beta R(t)} \right) \frac{dA'(t)}{2\pi} \qquad (4)$$

developed in reference 1 for bodies with discontinuous surface slopes is used.

The nose shock angle is determined from the assumption that, to first-order certainty, the shock bisects the free-stream characteristics and the body surface characteristics. With the use of equation (2), reference 1 gives

$$kF^2(y)\sqrt{r} = 2 \int_0^y F(y)\, dy \qquad (5)$$

as the condition satisfied along the nose shock. A similar treatment, also developed in reference 1, results in

$$\left.\begin{aligned} \int_{y_1}^{y_2} F(y)\, dy &= \frac{1}{2}(y_2 - y_1)\left[F(y_2) + F(y_1)\right] \\ y_2 - y_1 &= k\sqrt{r}\left[F(y_2) - F(y_1)\right] \end{aligned}\right\} \qquad (6)$$

as being the conditions which determine the positions of the trailing shocks.

Complete details of this "area balancing" technique are found in references 1 and 5. Notice that in equation (5) the difference between the value of the characteristic and the distance that the shock stands ahead of the Mach line from the nose (that is, $y - (x - \beta r)$) multiplied by the function $F(y)$ sets the value of the right-hand side of the equation which in this case is simply twice the integral of the $F(y)$ function. This particular feature also shows up in the improved equation for the location of the nose shock. Notice also that equations (2), (5), and (6) express the characteristic equation and the shock conditions as being functions primarily of distance and secondarily of body shape via the function $F(y)$.

An approximate near-field equation of the characteristic is obtained by applying the method of integration by parts to equation (1) in order to get an expression containing the function $F(y)$ and then by using some empirical simplifications to reduce that complex relationship even further. The equation that results from these operations is

$$y \approx x - \beta r + kF(y)\left[r^{1/2} - R^{1/2}(y)\right] + k\overline{F}(y)\left[R^{-1/2}(y) - r^{-1/2}\right] + L(y) \tag{7}$$

where

$$\overline{F}(y) = \int_0^y \frac{f(t)\,dt}{\sqrt{y - t}} = 2f(0)\sqrt{y} + \int_0^y F(y)\,dy \tag{8}$$

and

$$L(y) = 2M^2 f(0) \ln \left\{ \left[\frac{\sqrt{y + 2\beta r} + \sqrt{y}}{\sqrt{y + 2\beta r} - \sqrt{y}} \right] \left[\frac{\sqrt{y + 2\beta R(y)} - \sqrt{y}}{\sqrt{y + 2\beta R(y)} + \sqrt{y}} \right] \right\} \tag{9}$$

These expressions show that both the body radius $R(y)$ and the integral of the function $F(y)$ are significant factors in the near-field; $R(y)$ is the radius where a rearward running Mach line from y intersects the body surface and is found analytically or by numerical iteration from

$$\left.\begin{aligned} y &= x - \beta R(x) \\ R(y) &= R(x) \end{aligned}\right\} \tag{10}$$

Note also that the Whitham boundary condition $y = x - \beta r$ at $r = R$ from reference 1 is satisfied by equation (7).

The integral of the function $F(y)$ appears in equation (30) of reference 6 where it is seen to influence flow-field predictions even at large radial distances. It also is found in

a somewhat modified form in reference 7, which gives a method for extrapolating near-field pressure signatures to the mid- and far-field.

Numerical tests were performed to determine how well equation (7) approximated the behavior of equation (1) in the near-field, with a 5° cone taken as the test case. The results showed that through a Mach number range of 1.25 to 5.0 and a range of r/x from 0.09 to 0.17, equation (7) was sufficiently accurate to warrant the work necessary to develop a set of shock equations.

Using equation (7) and the shock bisection assumption gives

$$kF^2(y)\left[r^{1/2} - R^{1/2}(y)\right] + \bar{k}\bar{F}(y)\,F(y)\left[R^{-1/2}(y) - r^{-1/2}\right] + F(y)\,L(y)$$

$$= 2\int_0^y F(y)\,dy + \frac{k}{2}\int_0^y F^2(y)\,R'(y)\,R^{-1/2}(y)\,dy$$

$$+ \bar{k}\int_0^y \left[R^{-1/2}(y) - r^{-1/2}\right]\left[F'(y)\,\bar{F}(y) - F(y)\,\bar{F}'(y)\right]$$

$$+ \frac{\bar{k}}{2}\int_0^y F(y)\,\bar{F}(y)\,R'(y)\,R^{-3/2}(y)\,dy + \int_0^y \left[F'(y)\,L(y) - F(y)\,L'(y)\right]dy \qquad (11)$$

as the condition satisfied on the nose shock. Although complicated, equation (11) can be programed on a digital computer so that nose-shock solutions can be easily found.

A similar treatment with the intersecting characteristics originating on the body or wake surface and with some simplifying assumptions gives

$$\int_{y_1}^{y_2} F(y)\,dy + \frac{k}{4}\int_{y_1}^{y_2} F^2(y)\,R^{-1/2}(y)\,R'(y)\,dy$$

$$+ \bar{k}\int_{y_1}^{y_2}\left[F'(y)\,\bar{F}(y)\,R^{-1/2}(y)\right]dy + \frac{1}{2}\int_{y_1}^{y_2}\left[F'(y)\,L(y) - F(y)\,L'(y)\right]dy$$

$$= \frac{1}{2}(y_2 - y_1)\left[F(y_2) + F(y_1)\right] + \frac{k}{2}F(y_1)\,F(y_2)\left[R^{1/2}(y_2) - R^{1/2}(y_1)\right]$$

$$+ \frac{\bar{k}}{2}\left[\bar{F}(y_2)\,R^{-1/2}(y_2) + \bar{F}(y_1)\,R^{-1/2}(y_1)\right]\left[F(y_2) - F(y_1)\right]$$

$$+ \frac{1}{2}\left[L(y_1)\,F(y_2) - L(y_2)\,F(y_1)\right]$$

and

$$kF(y_1)\left[r^{1/2} - R^{1/2}(y_1)\right] + \bar{k}\bar{F}(y_1)\left[R^{-1/2}(y_1) - r^{-1/2}\right] + L(y_1) - y_1$$

$$= kF(y_2)\left[r^{1/2} - R^{1/2}(y_2)\right] + \bar{k}\bar{F}(y_2)\left[R^{-1/2}(y_2) - r^{-1/2}\right] + L(y_2) - y_2 \qquad (13)$$

as the governing conditions on the trailing shocks. An examination of equation (12) shows that "area balancing" is the core of the solution; area balancing for the improved method is represented by equation (11), with only the first term on the right-hand side being kept and used, and by equation (12) reduced to

$$\int_{y_1}^{y_2} F(y)\,dy = \frac{1}{2}(y_2 - y_1)\left[F(y_2) + F(y_1)\right]$$

The other terms in equations (11) and (12) are combinations of body radius, surface slope, $F(y)$, and free-stream Mach number which serve to shift the shock location forward or rearward from the location established by the simple area balancing solution. A comparison of the area balancing method and the shock equation method is made at the end of the next section.

RESULTS AND COMPARISONS

Four bodies of revolution are used to compare wind-tunnel data, near-field theory, and the improved near-field method: a cone-cylinder model, a model with a linear-area forebody and a cylindrical afterbody, a model with a "lower bound" (ref. 8) forebody and a cylindrical afterbody, and a truncated cone-cylinder ducted-nacelle model. Although the wind-tunnel models are of finite size, semi-infinite mathematical representations are used in the computer program. The pressure disturbances from the model sting are excluded from the signatures, so the wind-tunnel models are, in effect, also semi-infinite.

The flow-field pressures are calculated from

$$\frac{\Delta p}{p} = \frac{\gamma M^2 F(y)}{\sqrt{2\beta r}} \qquad (14)$$

(which was obtained from ref. 1) so that a direct comparison between near-field theory and the improved near-field method can be made. Since most of the data are obtained from a sonic-boom report (ref. 4), the measured signatures and the near-field theory signatures are shifted so that they are alined with the improved-method signatures in the same

manner and for the same reason as in reference 4. Also, similar dimensionless pressure and length parameters are employed to avoid confusion and aid direct comparison.

The following order is used to present and discuss the models, test data, and theoretical predictions: (1) cone-cylinder model, (2) linear-area and "lower bound" models, (3) ducted-nacelle model, and (4) comparison of the area balancing and the shock equation solutions of nose-shock location.

Cone-Cylinder Model

Flow-field pressures are calculated for the lowest-fineness-ratio cone-cylinder body in reference 4 (see model 1 in fig. 1) and are presented in dimensionless parameter form in figure 2. This body, for which the ratio of the semivertex angle to the Mach angle is the largest in the cone-cylinder series at all Mach numbers, constitutes the most severe test of the improved near-field method. Mach numbers of 2.96, 3.83, and 4.63 and values of r/l of 2.0 and 5.0 are used to compare the experimental data and theoretical predictions (see fig. 2). No boundary-layer displacement thickness is added to the body radius because a complete and accurate knowledge of the flow over this as well as the other bodies of revolution used in this report is not available.

At Mach numbers of 2.96 and 3.83 with $\frac{r}{l} = 5.0$, the predictions from the improved near-field method compare well with wind-tunnel data (see figs. 2(a) and 2(b)). Peak predicted overpressures are higher than measured overpressures possibly because of the rounding effects of wind-tunnel turbulence and model vibration, but nose-shock location and signature shape show the differences caused by the extra terms in the equation of the characteristic (eq. (7)).

Agreement between experiment and prediction is less complete at $M = 4.63$ with r/l values of 5.0 and 2.0 (see figs. 2(c) and 2(d)). At this Mach number the ratio of cone semivertex angle to Mach angle is 0.516; this value is above what is considered the limit of linearized theory. Nevertheless, the improved near-field method does provide the better solution and picture of what is happening in the flow field. Particularly interesting is the fact that no distinct trailing shock is measured or predicted by the improved method at the test Mach numbers and at the distances selected for measurement. This feature is probably due to the slow coalescence of the body characteristics in the region of the shoulder plus the tendency for wind-tunnel turbulence and model vibration to smear out the recording of any small shocks that might have formed. Signatures with nose shocks but without trailing shocks are also presented for the other models in this report.

Linear-Area and "Lower Bound" Models

In addition to the cone-cylinder model, figure 1 also shows the next two models (from ref. 4) which were used for flow-field comparisons. Like model 1, models 2 and 3 have

the lowest fineness ratio in their respective series in reference 4. Since they are blunt $\left(R'(0) \geq \frac{1}{\beta}\right)$, a somewhat different treatment must be used to get flow-field information.

When a blunt body is "Mach sliced" in order to determine its disturbance-oriented area distribution and therefore its source strength function, it is found that the sources begin at an initial value of $x_o = x_\beta - \beta R_\beta$, as shown in figure 3. As the Mach planes move rearward between $x = x_o$ and $x = 0$, the areas intercepted are entirely on one side of the body axis. Body radii R_f and R_i are the maximum and minimum values on the meridian section shown in figure 3(a). However, the derivation of equation (4) assumes that only one intersection exists, so the nose is suitably modified to make the theory applicable over the entire length of the body.

The method that gives good results, that is consistent over the Mach number range described, and that is plausible in concept is shown in figure 3(b). A tangent cone with its apex at $x_t = x_o - x_\beta = -\beta R_\beta$ is used to start the new representative body of revolution. Figure 3(c) shows the components of the $F(y)$ calculation and how those of the representative body (blunt body with tangent cone) compare with corresponding values of the blunt body.

A point in the flow field cannot "feel" the influence along Mach or characteristic lines of a disturbance from the nose of the blunt body because of the shielding that is provided by the nose itself. Any initial disturbance experienced appears to originate from sources ahead of the nose. Therefore, putting sources (body volume) in a tangent cone does not change the flow-field representation if the new function $F(y)$ has approximately the same shape and, more importantly, the same integrated area as the blunt body, as is shown in figure 3(c).

This tangent-cone method insures that $R'(y)$ is finite everywhere, that $R(y)$ has a single value everywhere, and that the distance to the tangent cone apex x_o is fixed by body geometry and Mach number considerations only. The results from using this method on models 2 and 3 are shown in figures 4 and 5.

It can be seen that the wind-tunnel data and the theoretical predictions compare less favorably as bluntness and Mach number increase, but that for a body of moderate bluntness (model 2) the improved near-field method does reasonably well over the Mach number range covered by the tests.

A convergence test of the tangent-cone method (based on varying $\Delta l/l$) is shown in figure 6. Model 3 was used, with $M = 4.63$ and $\frac{r}{l} = 5.0$ as the test conditions. The reference line of 1.0 is set for $\frac{\Delta l}{l} = 0.02$ because the number of area stations used to describe the forebody is large (51) but not excessive.

The lines drawn between the circled points in figure 6 are trend indicators rather than loci of values and are used to show that for this blunt model, Mach number, and radial

distance, a very large number of area stations are needed to reach convergence. Most of the scatter in the maximum-pressure-ratio data points is due to the effect of small differences in the individual F(y) functions. The steep pressure gradient following the nose shock coupled with the numerical technique used in solving the nose-shock equation magnifies these differences and causes the observed behavior. However, the integral of the positive lobe of the F(y) function (the shaded area shown in the inset sketch) is much more stable. When the pressure signatures for which $\frac{\Delta l}{l} \leqq 0.01$ are overlaid, scarcely any difference can be seen. If the one data point at $\frac{\Delta l}{l} = 0.01333$ is excluded, the useful range could be extended to $\frac{\Delta l}{l} \leqq 0.02$. Thus, while a value of $\frac{\Delta l}{l} \leqq 0.004$ is needed to produce the most accurate solution, $\frac{\Delta l}{l} = 0.02$ gives a satisfactory and usable one. For this reason, a value of $\frac{\Delta l}{l}$ of 0.02 is used to obtain pressure signatures for both blunt bodies in this report.

Ducted-Nacelle Model

Figure 7 shows the ducted-nacelle model used in reference 9. The equation of the characteristic used in that reference and in that application was

$$y = x - \beta r + kF(y)\left[r^{1/2} - R^{1/2}(0)\right] \tag{15}$$

The area balancing technique of references 1, 5, and 9 was used to locate the shocks in the flow field surrounding the nacelle.

It is interesting that both the method used in reference 9 and the improved near-field method do equally well in predicting nose-shock location and strength, as is seen in figure 8. However, the pressure gradient in the flow field caused by the shoulder on the nacelle is better predicted by the improved method, even at M = 2.96.

Comparison of Shock-Location Methods

Figure 9 shows a comparison of the nose-shock locations and strengths calculated by the area balancing method and by the shock equation method. The same form of the characteristic (eq. (7)) is used to predict the nonshock part of the pressure signature.

With the exceptions of the very blunt model 3 and the ducted-nacelle model (see signatures in figs. 9(c) and 9(d)), there seems to be little justification in favoring one method over the other. However, these exceptions point out the factors which alter the area balancing prediction.

The nose shock on the ducted-nacelle model starts out at the lip strongly two dimensional in angle and strength, whereas on model 3 it is theoretically a strong detached bow shock. In both these cases, the effects of radius, surface slope, and fineness ratio are

very pronounced. Therefore, it would seem that the area balancing method is applicable only to bodies of revolution with conical nose sections.

CONCLUDING REMARKS

An improved near-field method for calculating the pressure disturbances in the supersonic flow field about a body of revolution has been presented and discussed. Comparisons of the predictions of the improved method with wind-tunnel data and Whitham's theory have been made with the use of three closed-nose bodies of revolution and one ducted body of revolution at Mach numbers of 2.96, 3.83, and 4.63. It has been demonstrated that reasonably good flow-field predictions can be made with this improved method; thus the increased complexity in the system of equations used to predict the pressure signatures by this method is justified. Although emphasis has been placed on sonic boom (because experimental data were so readily available), the improved method is applicable to the calculation of near-field supersonic-flow properties about pointed or ducted bodies of revolution.

Langley Research Center,
National Aeronautics and Space Administration,
Hampton, Va., August 24, 1971.

REFERENCES

1. Whitham, G. B.: The Flow Pattern of a Supersonic Projectile. Commun. Pure Appl. Math., vol. V, no. 3, Aug. 1952, pp. 301-348.

2. Carlson, Harry W.; Mack, Robert J.; and Morris, Odell A.: A Wind-Tunnel Investigation of the Effect of Body Shape on Sonic-Boom Pressure Distributions. NASA TN D-3106, 1965.

3. Carlson, Harry W.: Correlation of Sonic-Boom Theory With Wind-Tunnel and Flight Measurements. NASA TR R-213, 1964.

4. Shrout, Barrett L.; Mack, Robert J.; and Dollyhigh, Samuel M.: A Wind-Tunnel Investigation of Sonic-Boom Pressure Distributions of Bodies of Revolution at Mach 2.96, 3.83, and 4.63. NASA TN D-6195, 1971.

5. Middleton, Wilbur D.; and Carlson, Harry W.: A Numerical Method For Calculating Near-Field Sonic-Boom Pressure Signatures. NASA TN D-3082, 1965.

6. Landahl, M.; Ryhming, I.; and Lofgren, P.: Nonlinear Effects on Sonic Boom Intensity. Third Conference on Sonic Boom Research, Ira. R. Schwartz, ed., NASA SP-255, 1971, pp. 3-15.

7. Pan, Y. S.: Application of Whitham's Theory to Sonic Boom in the Mid- or Near-Field. AIAA J., vol. 8, no. 11, Nov. 1970, pp. 2080-2082.

8. Jones, L. B.: Lower Bounds for Sonic Bangs. J.R.A.S. (Tech. Notes), vol. 65, no. 606, June 1961, pp. 433-436.

9. Mack, Robert J.: A Numerical Method For Evaluation and Utilization of Supersonic Nacelle-Wing Interference. NASA TN D-5057, 1969.

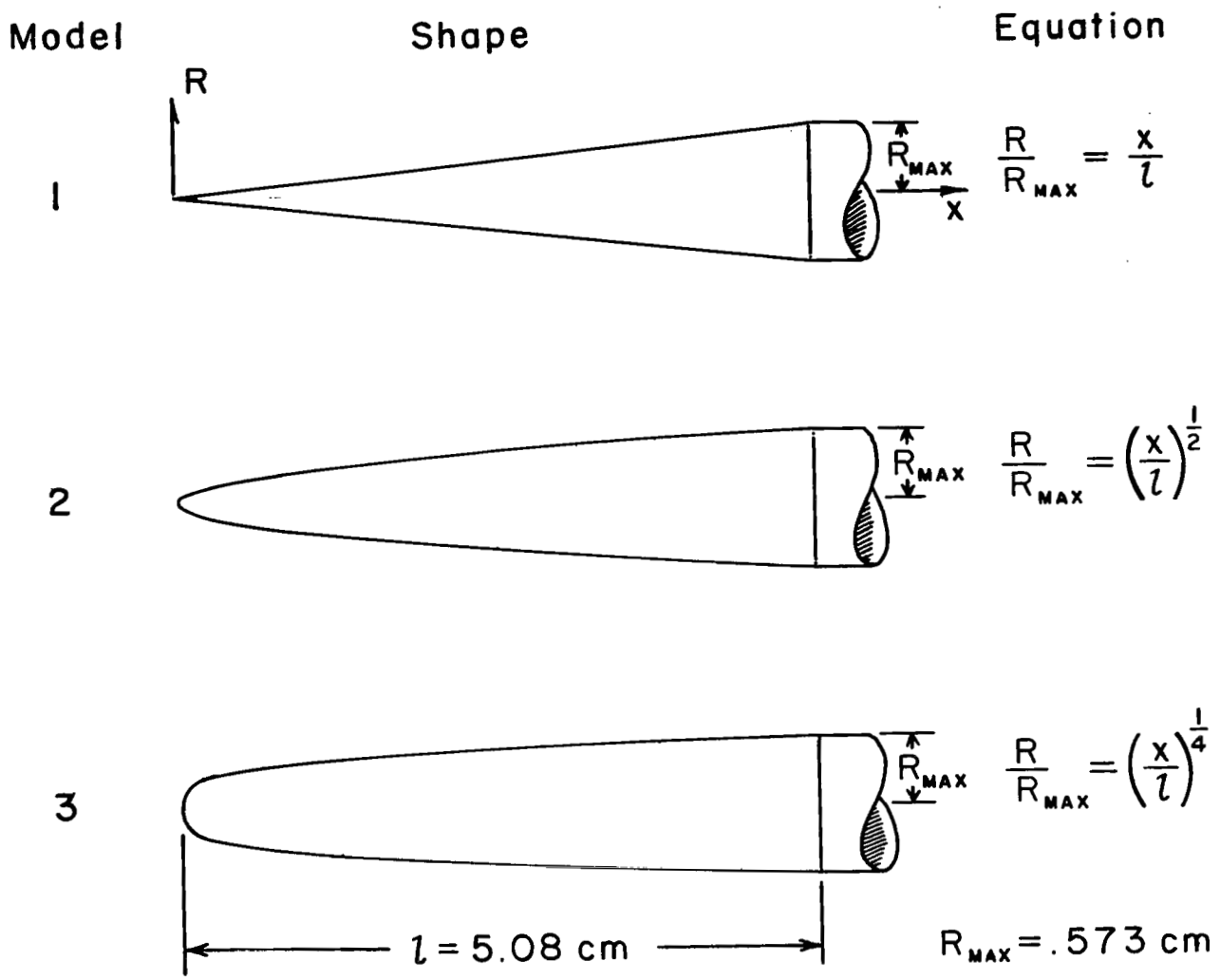

Figure 1.- Closed-nose bodies of revolution (from ref. 4).

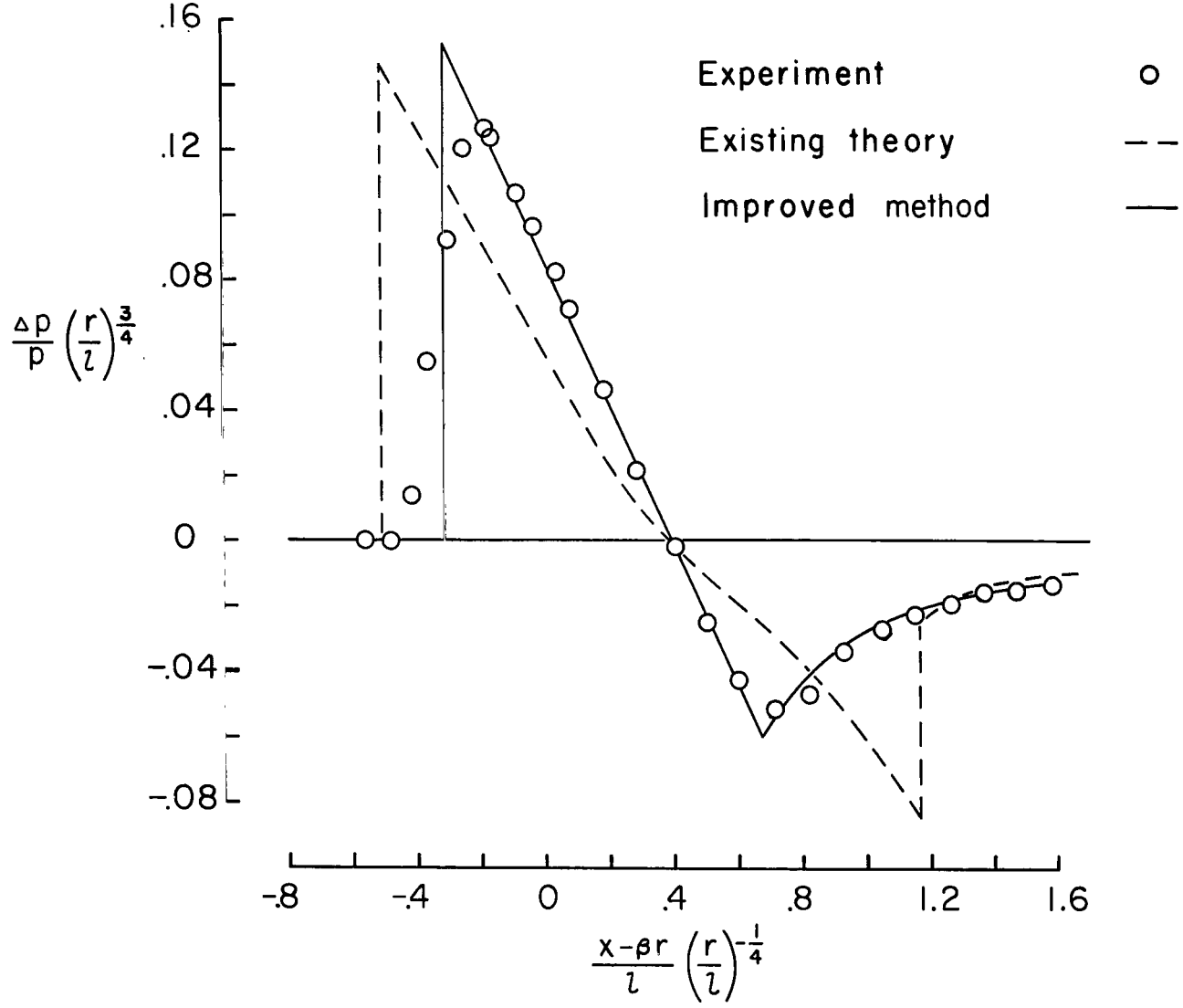

(a) M = 2.96; $\frac{r}{l} = 5.0$.

Figure 2.- Pressure distributions in the flow field of model 1. (Experimental data taken from ref. 4.)

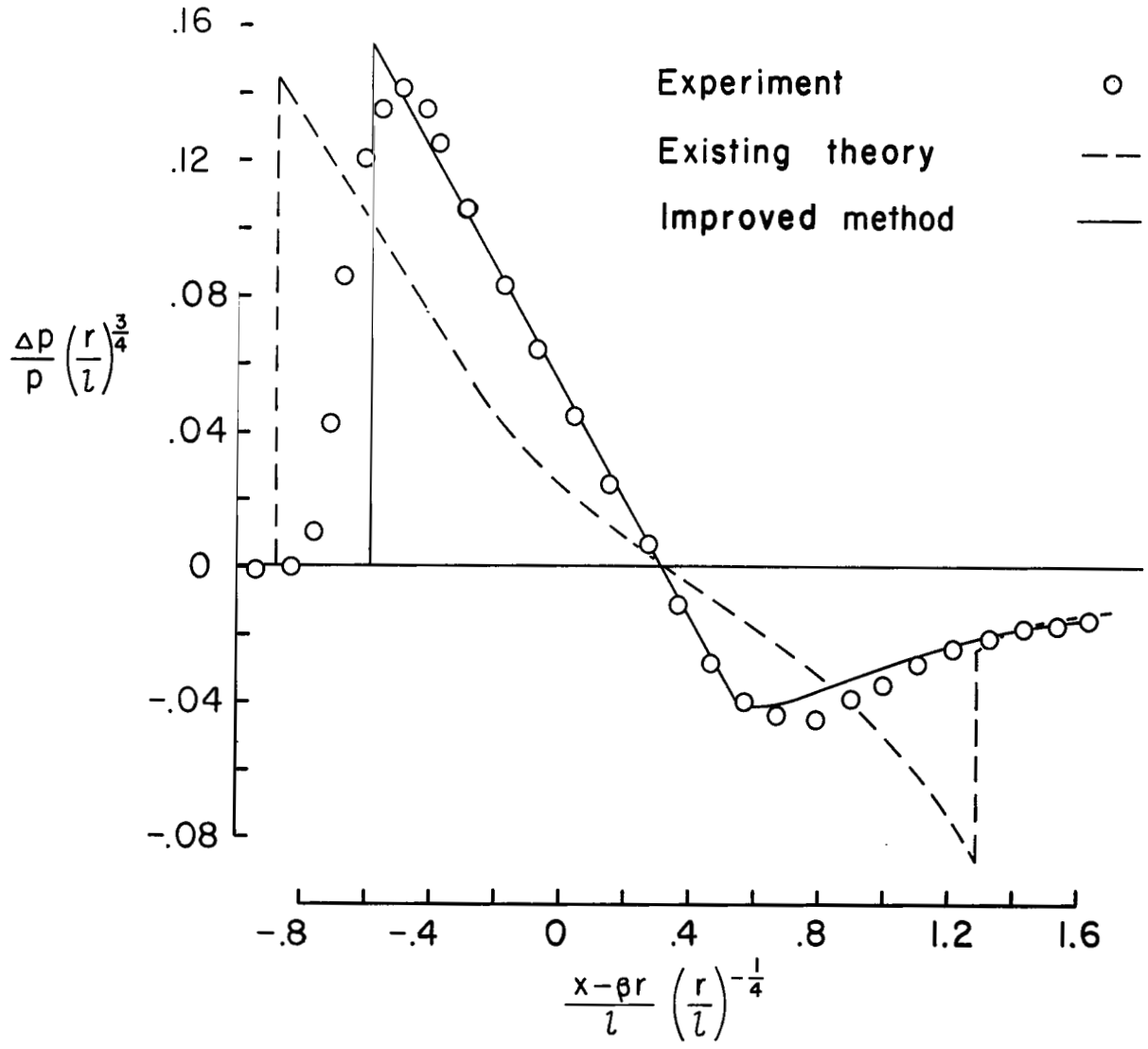

(b) M = 3.83; $\frac{r}{l} = 5.0$.

Figure 2.- Continued.

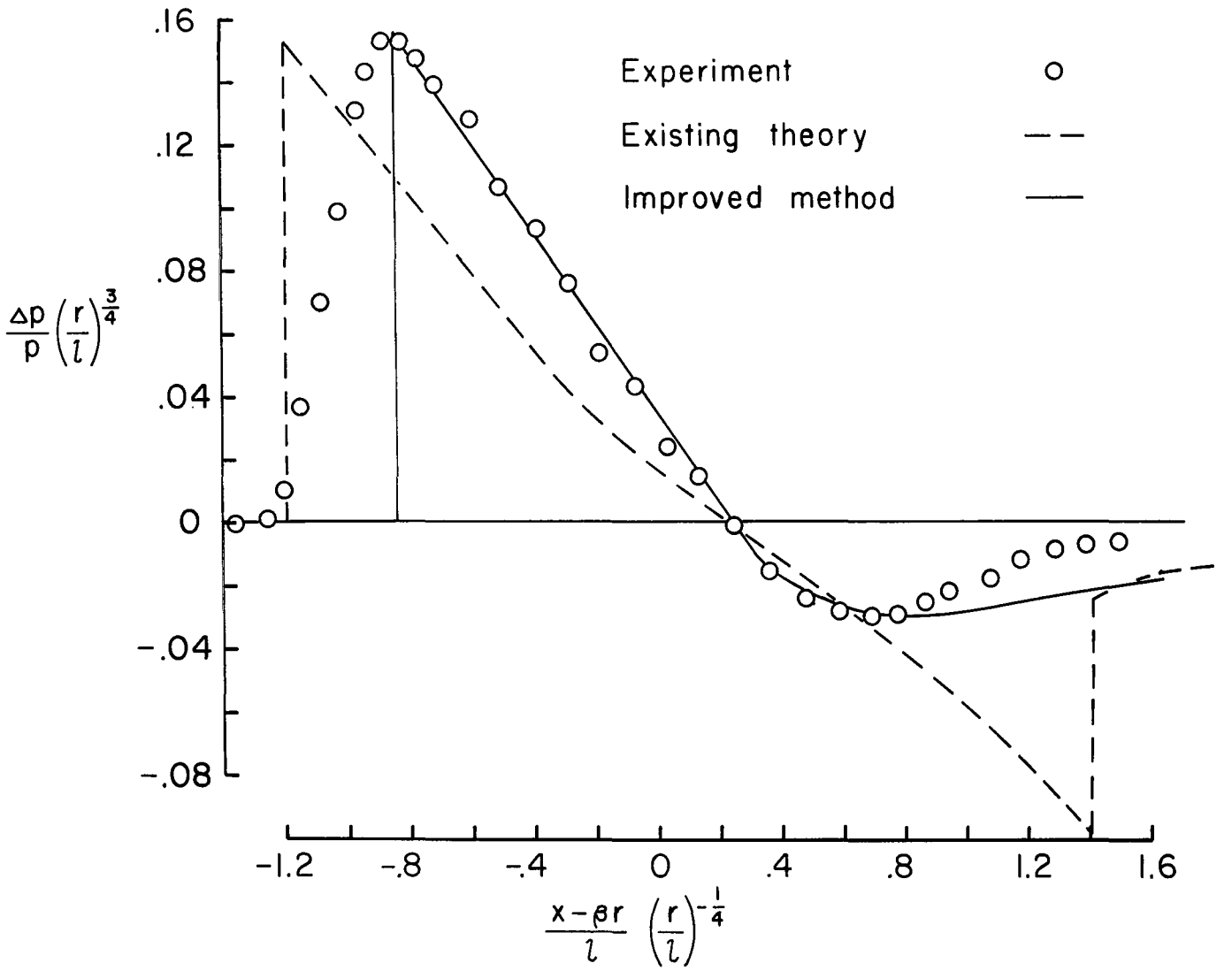

(c) M = 4.63; $\frac{r}{l} = 5.0$.

Figure 2.- Continued.

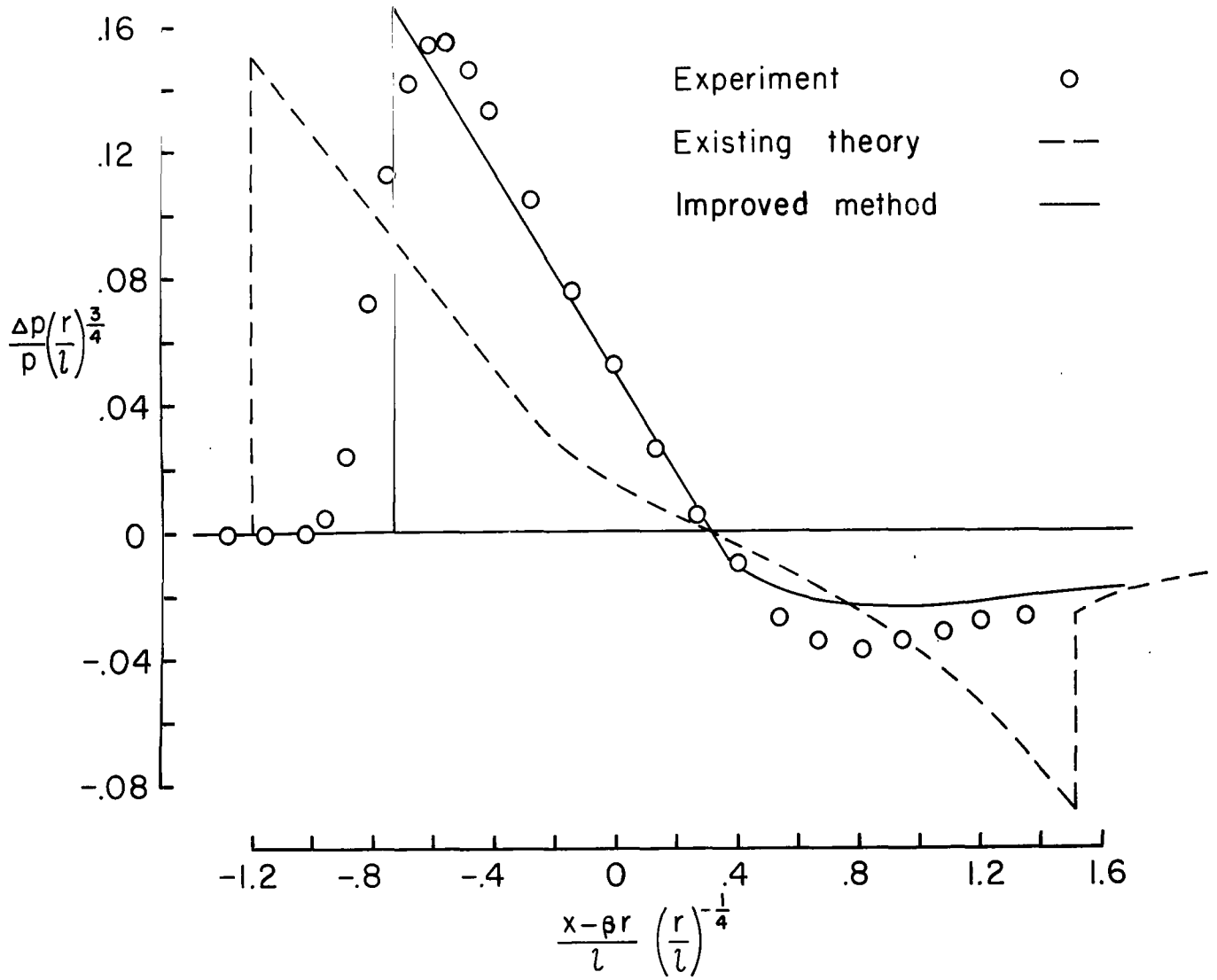

(d) $M = 4.63$; $\frac{r}{l} = 2.0$.

Figure 2.- Concluded.

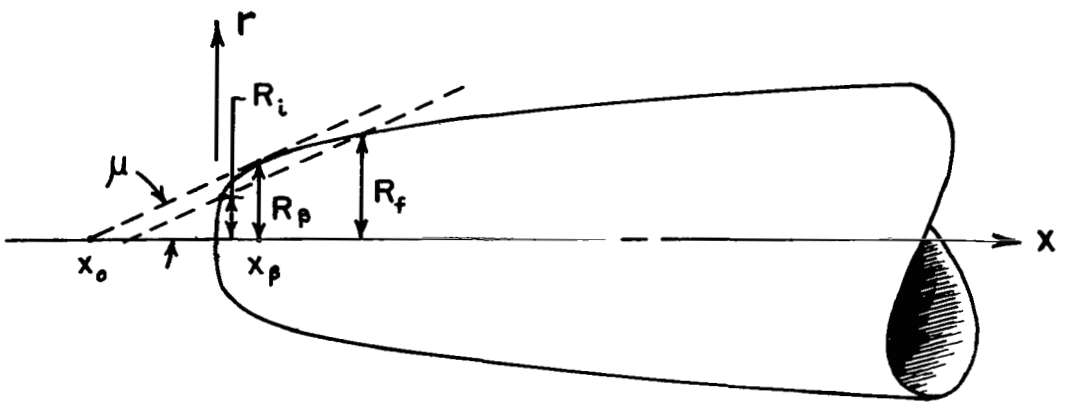

(a) Blunt-body geometry.

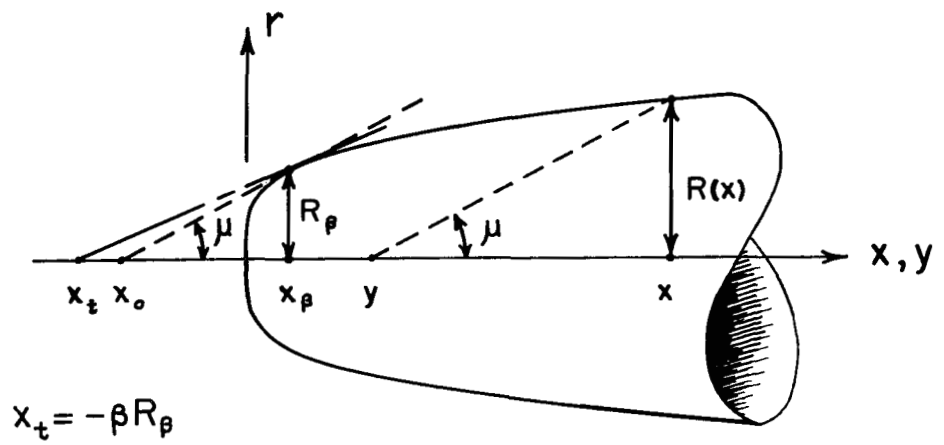

$$x_t = -\beta R_\beta$$

$$y = x - \beta R(x)$$

$$R(y) = R(x)$$

$$R'(y) = \lim_{\Delta y \to 0} \frac{R(y+\Delta y) - R(y)}{\Delta y}$$

(b) Schematic of tangent cone.

Figure 3.- Method of modifying blunt bodies for application of linearized theory

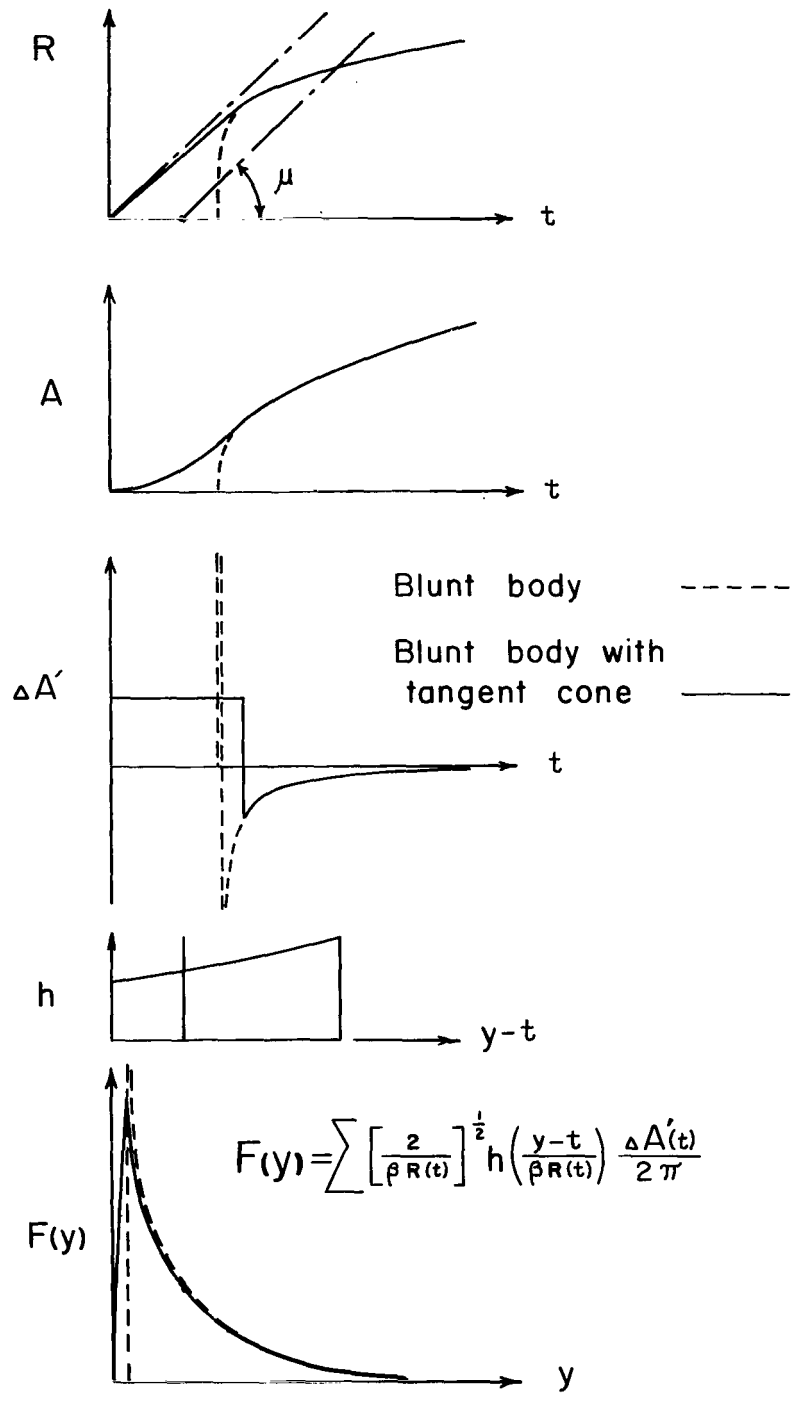

(c) Sketch of F(y) calculation factors.

Figure 3.- Concluded.

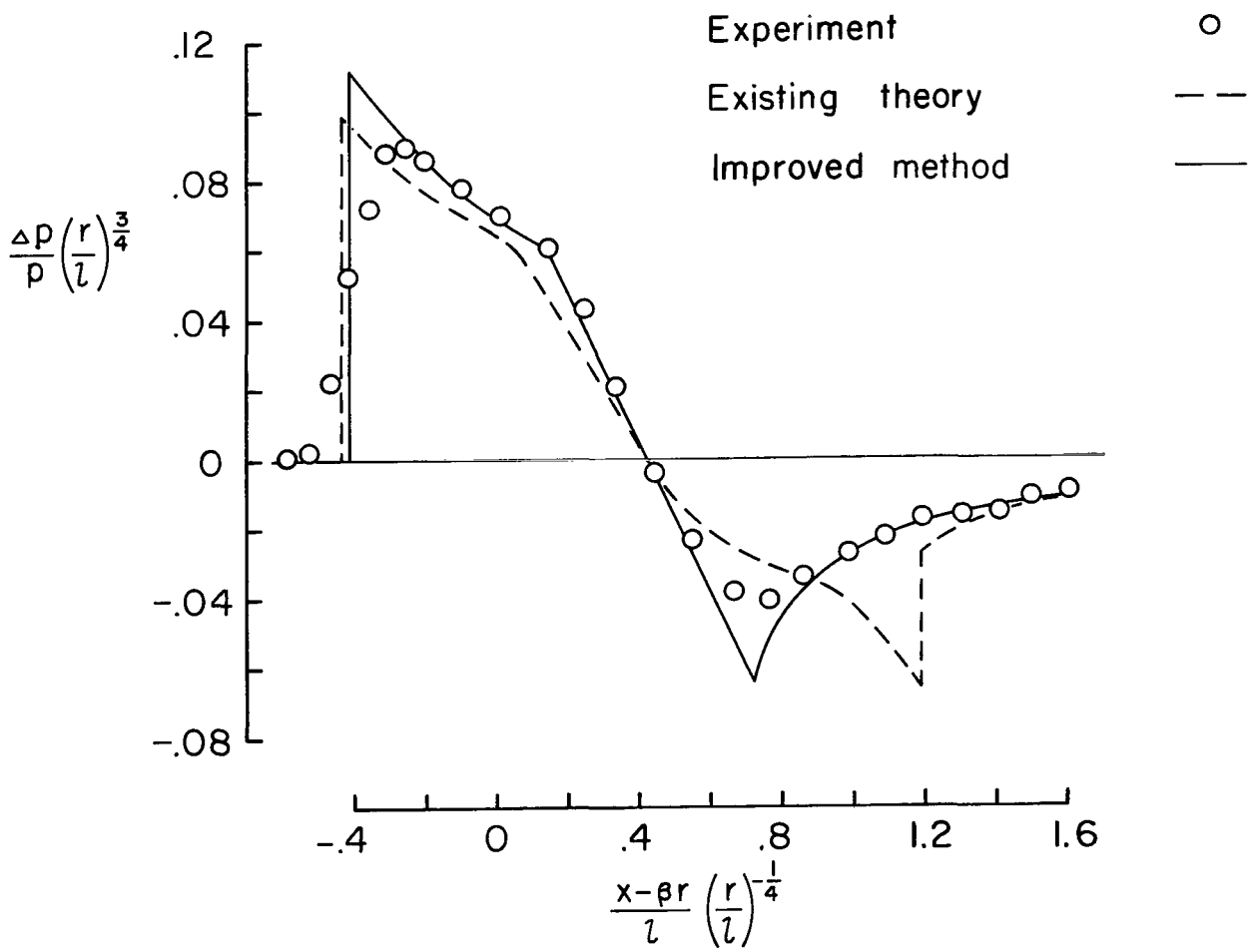

(a) M = 2.96; $\frac{r}{l} = 5.0$.

Figure 4.- Pressure distributions in the flow field of model 2.
(Experimental data taken from ref. 4.)

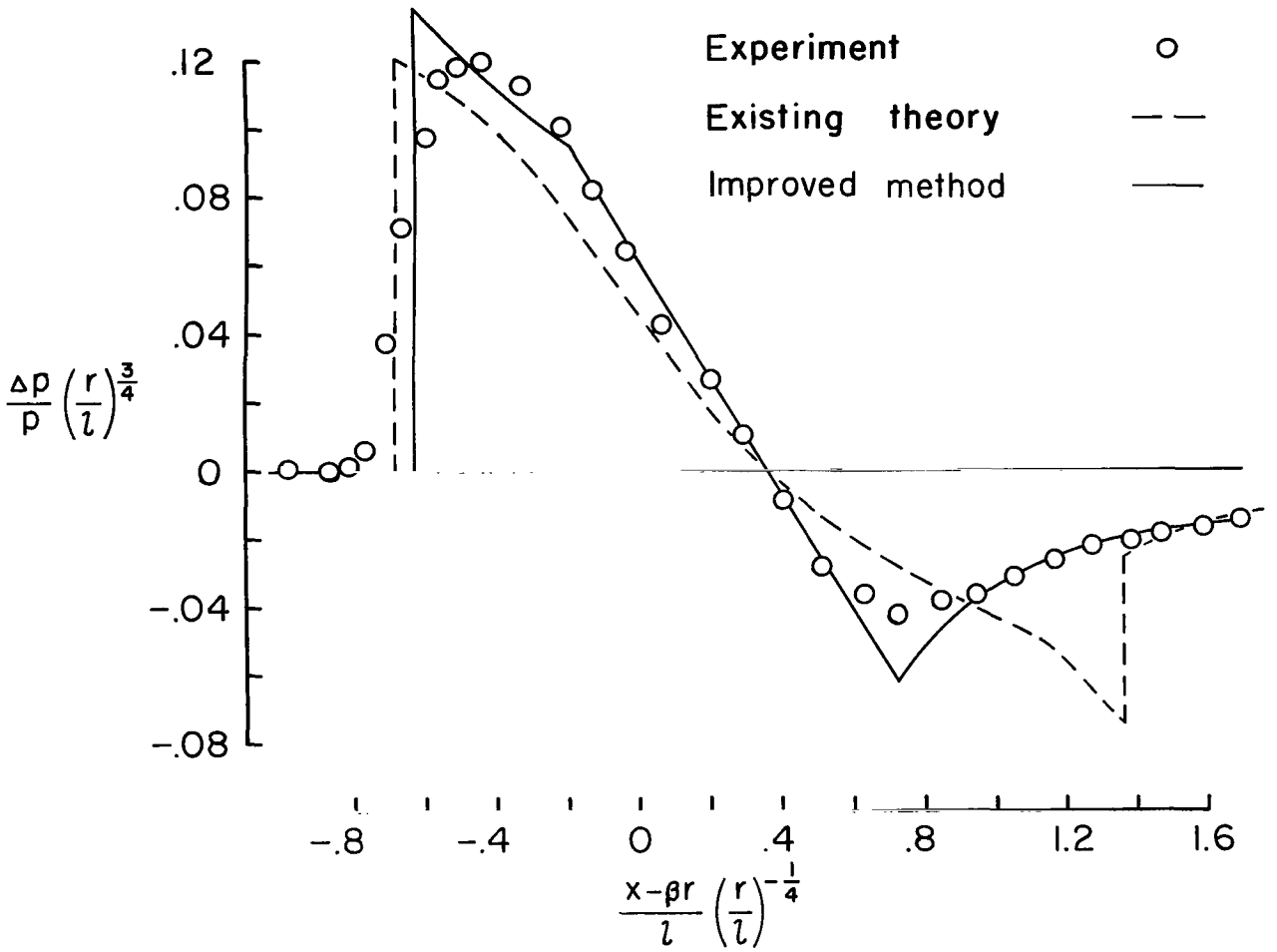

(b) M = 3.83; $\frac{r}{l}$ = 5.0.

Figure 4.- Continued.

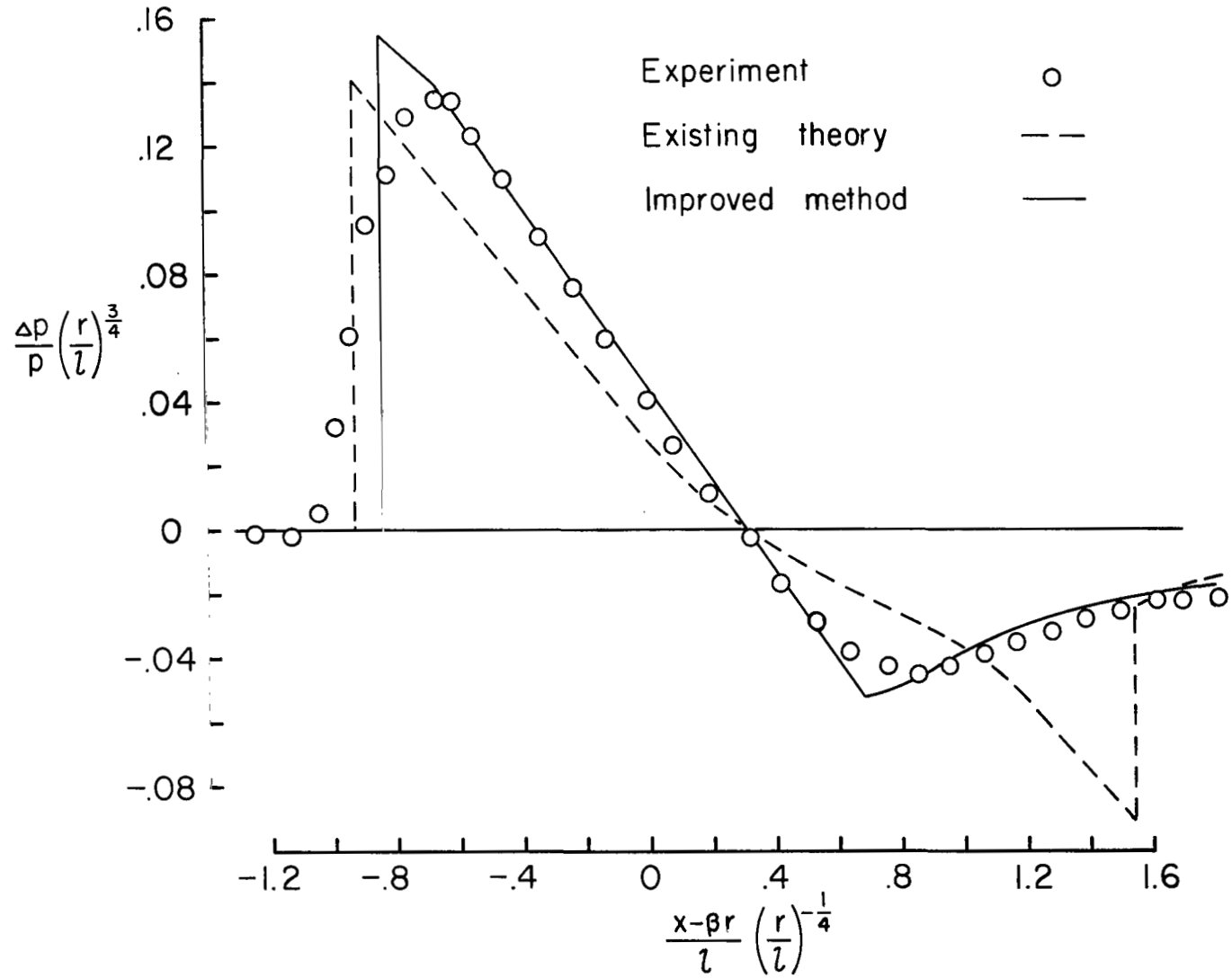

(c) M = 4.63; $\frac{r}{l} = 5.0$.

Figure 4.- Continued.

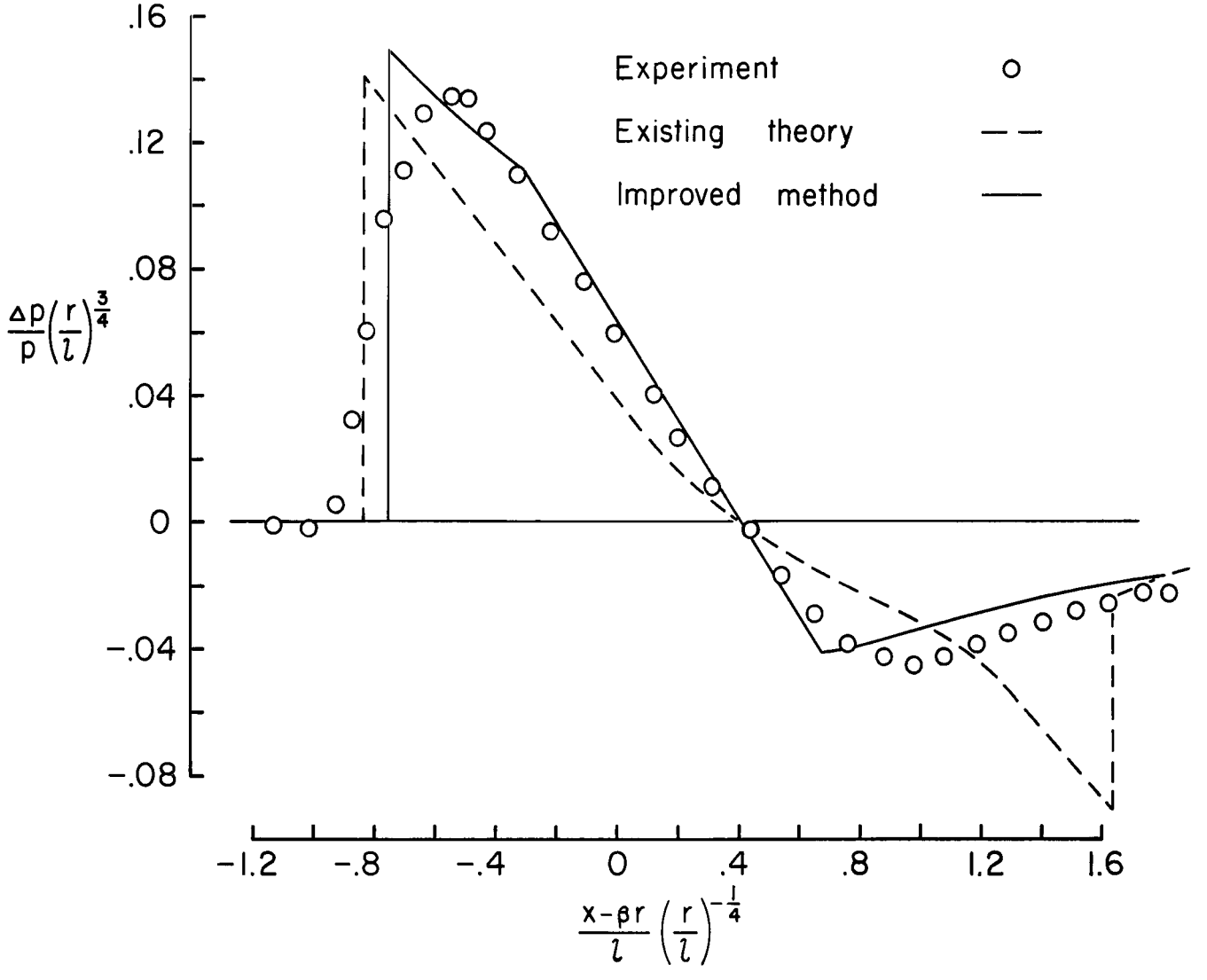

(d) M = 4.63; $\frac{r}{l} = 2.0$.

Figure 4.- Concluded.

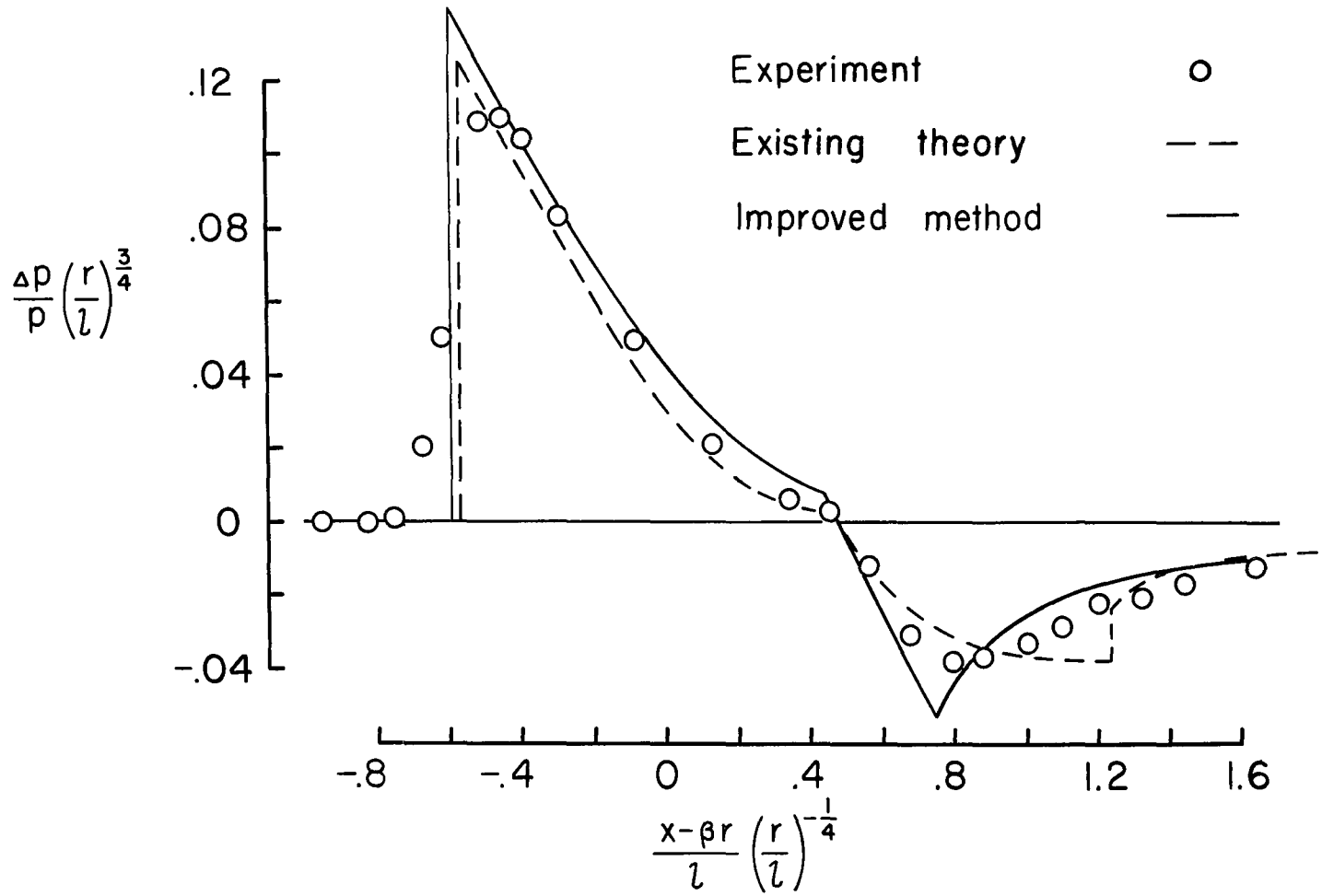

(a) $M = 2.96$; $\frac{r}{l} = 5.0$.

Figure 5.- Pressure distributions in the flow field of model 3. (Experimental data taken from ref. 4.)

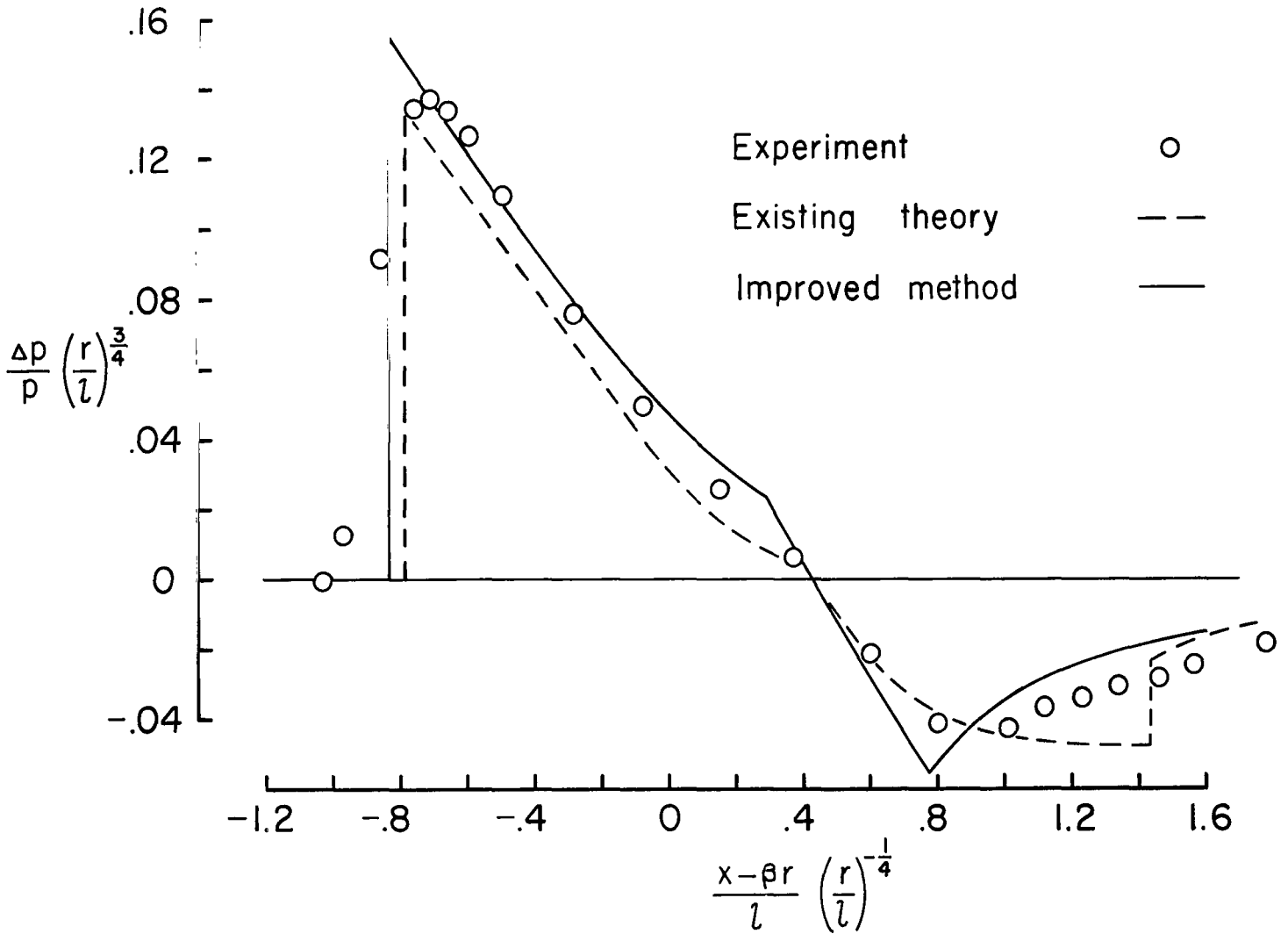

(b) M = 3.83; $\frac{r}{l} = 5.0$.

Figure 5.- Continued.

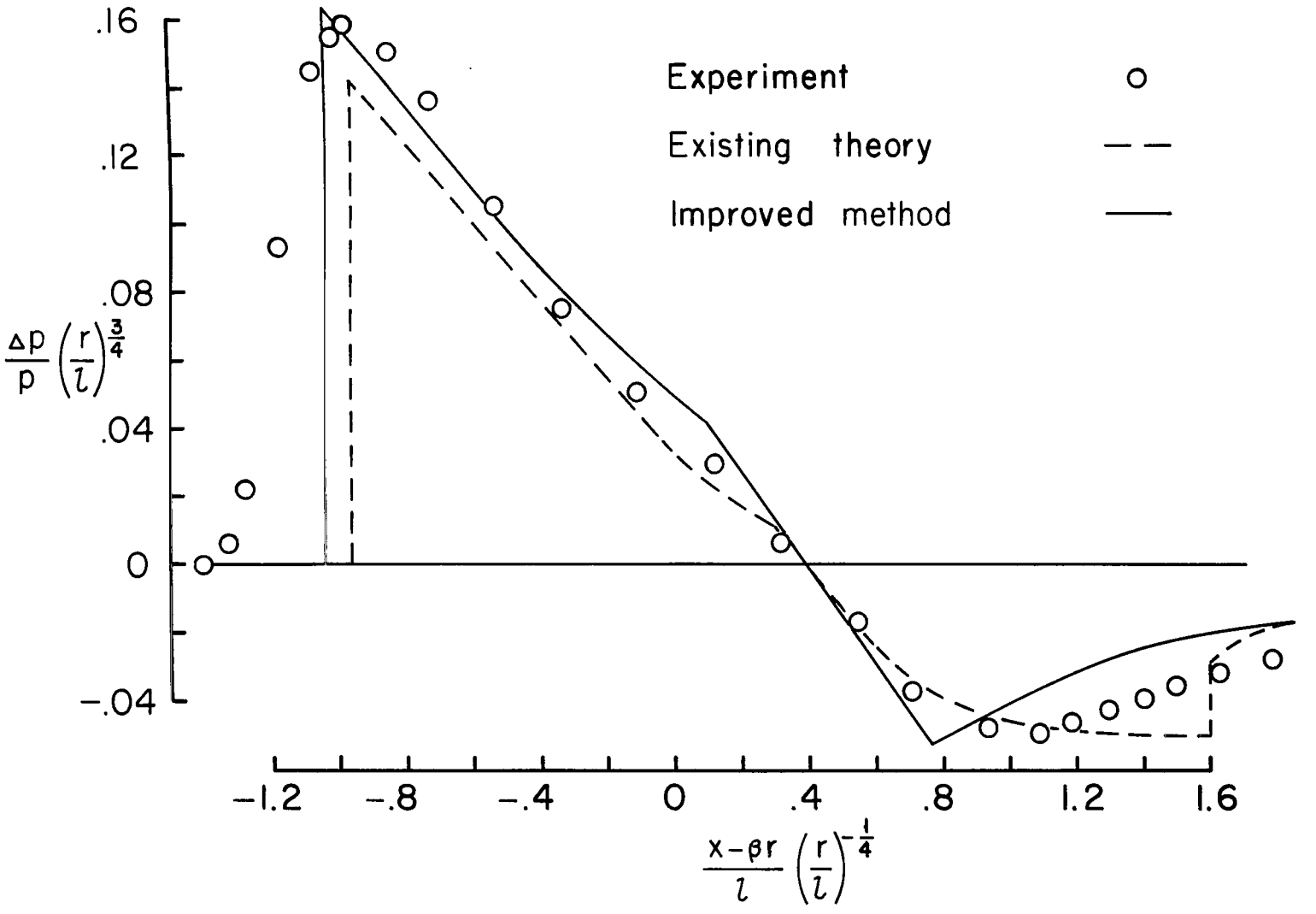

(c) $M = 4.63$; $\frac{r}{l} = 5.0$.

Figure 5.- Continued.

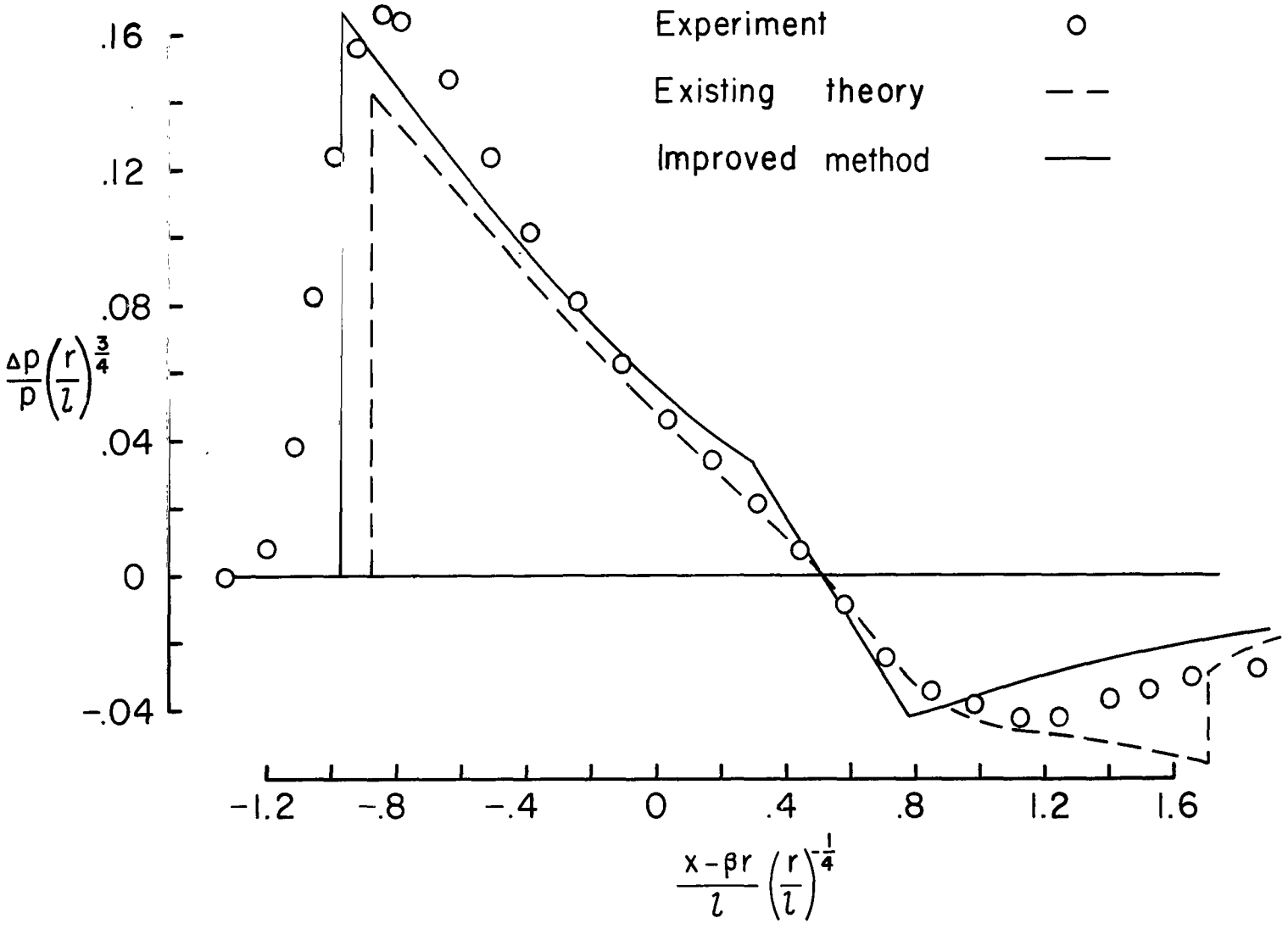

(d) $M = 4.63$; $\frac{r}{l} = 2.0$.

Figure 5.- Concluded.

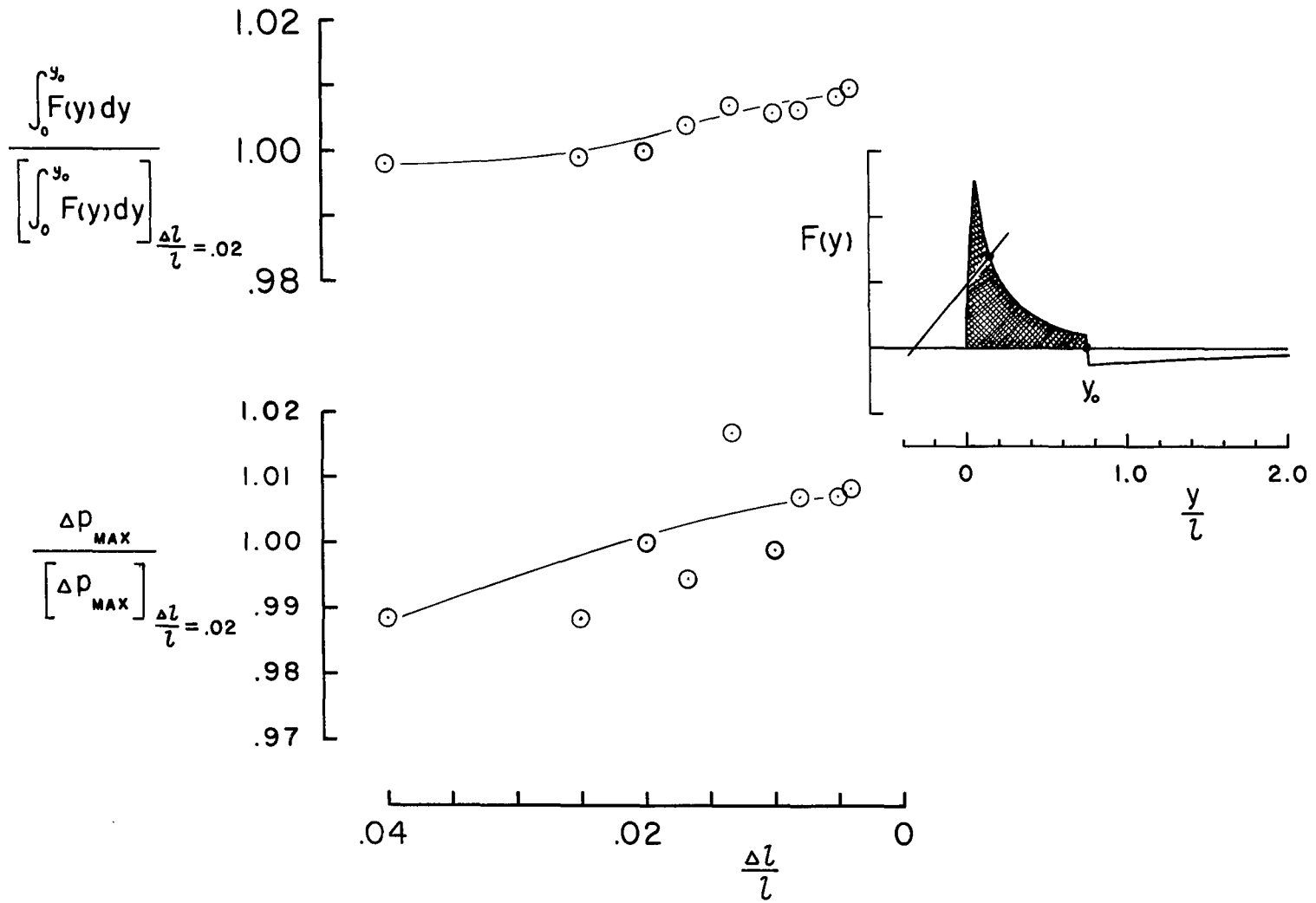

Figure 6.- Convergence test results obtained from model 3 at $M = 4.63$ and $\frac{r}{l} = 5.0$.

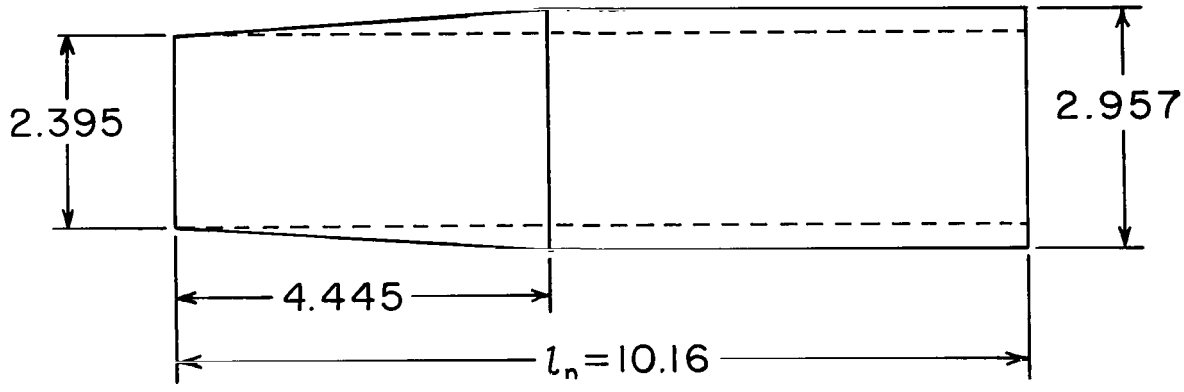

Figure 7.- Ducted-nacelle model (from ref. 9). (All dimensions are in cm.)

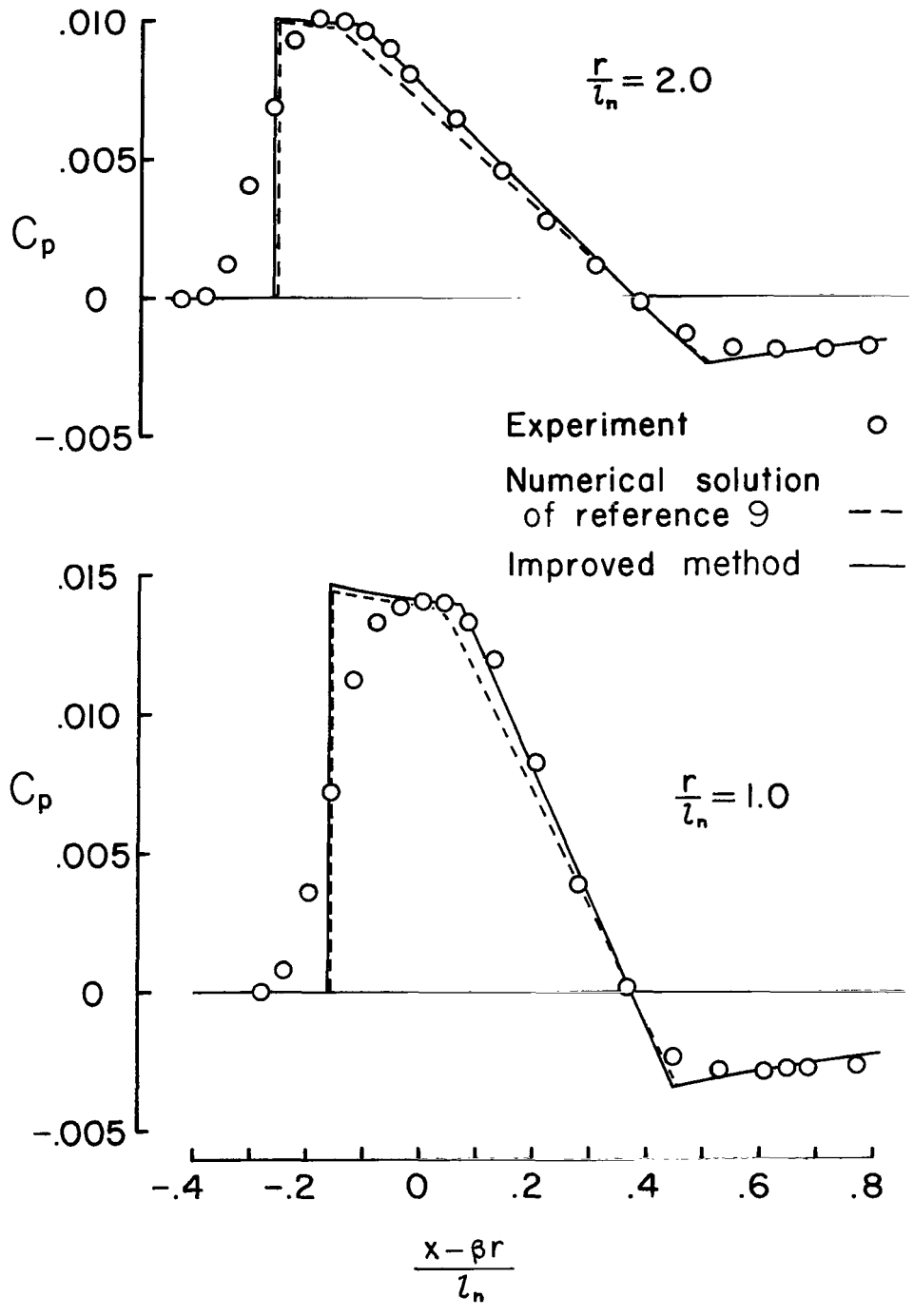

Figure 8.- Pressure distributions in the flow field of the ducted-nacelle model at M = 2.96. (Model and experimental data from ref. 9.)

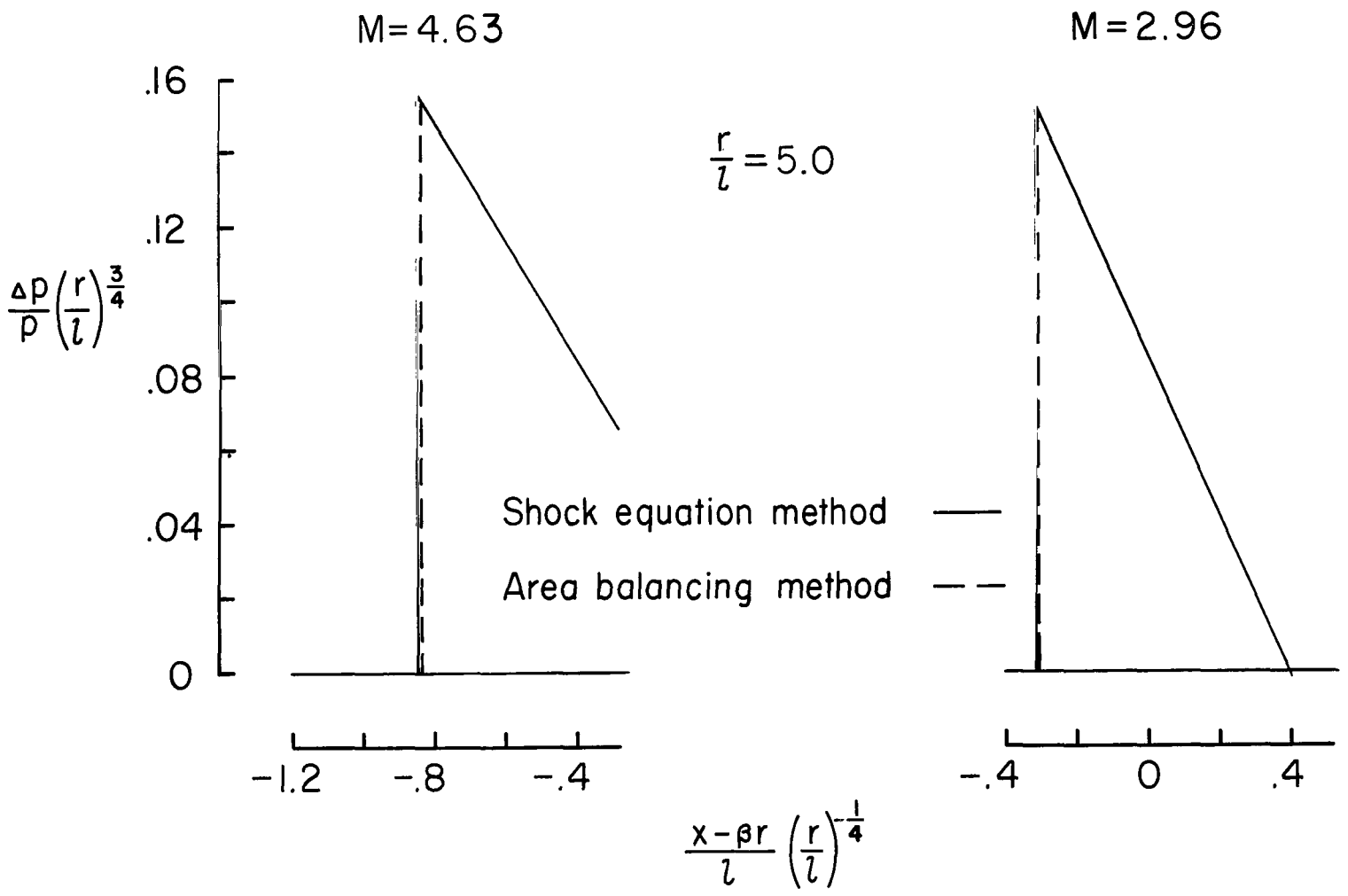

(a) Model 1.

Figure 9.- Comparison of theoretical nose-shock location and strength.

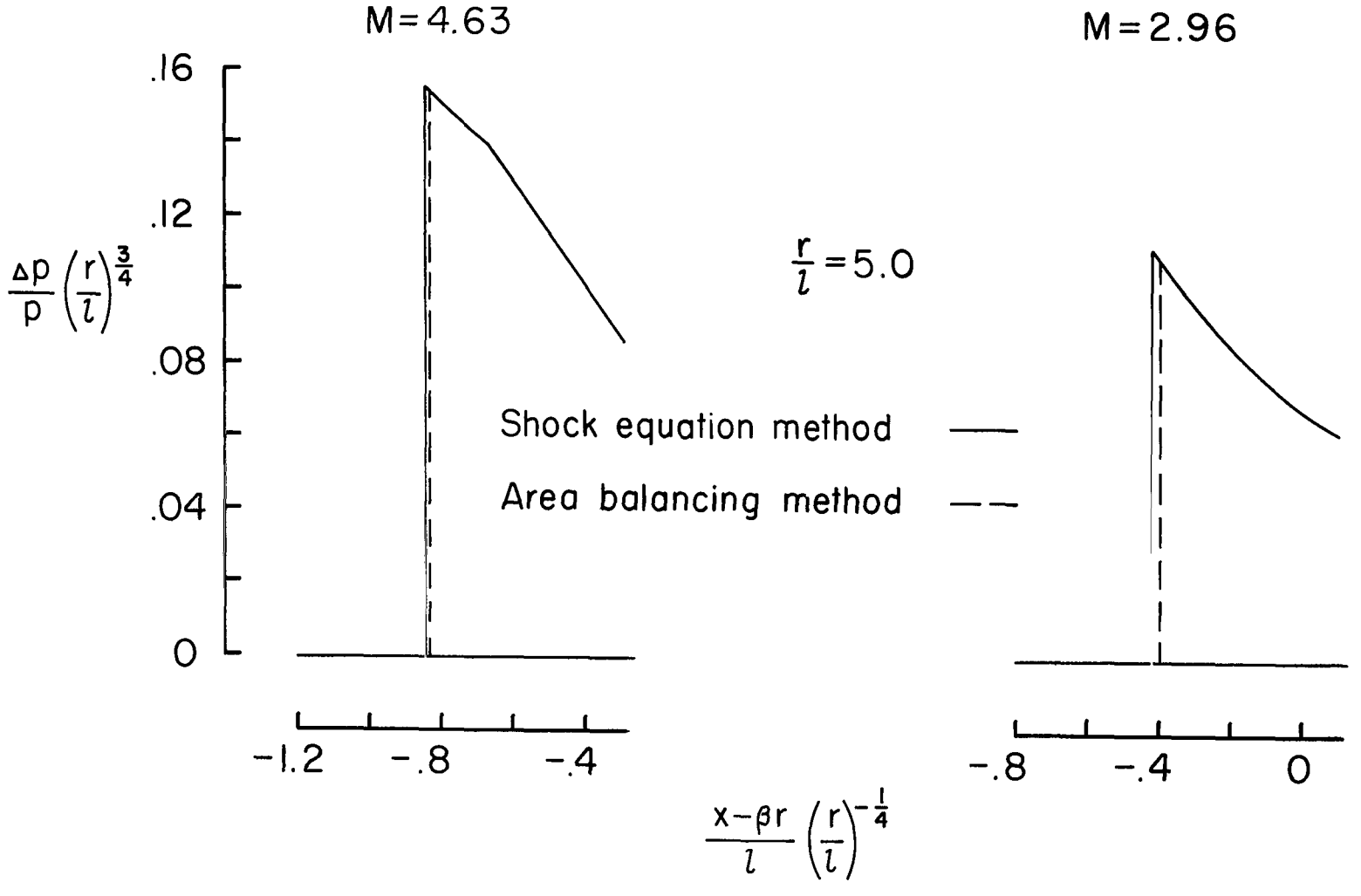

(b) Model 2.

Figure 9.- Continued.

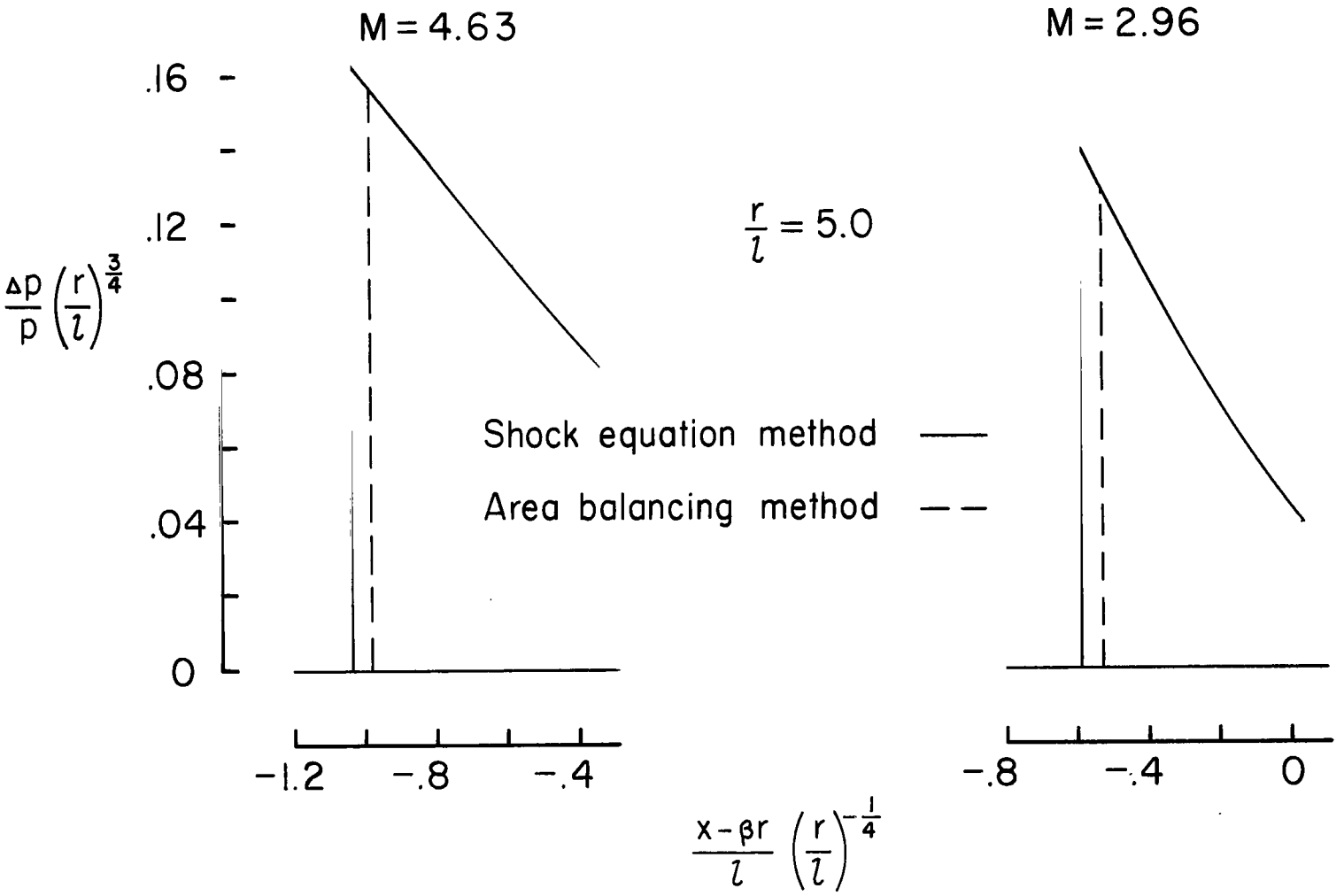

(c) Model 3.

Figure 9.- Continued.

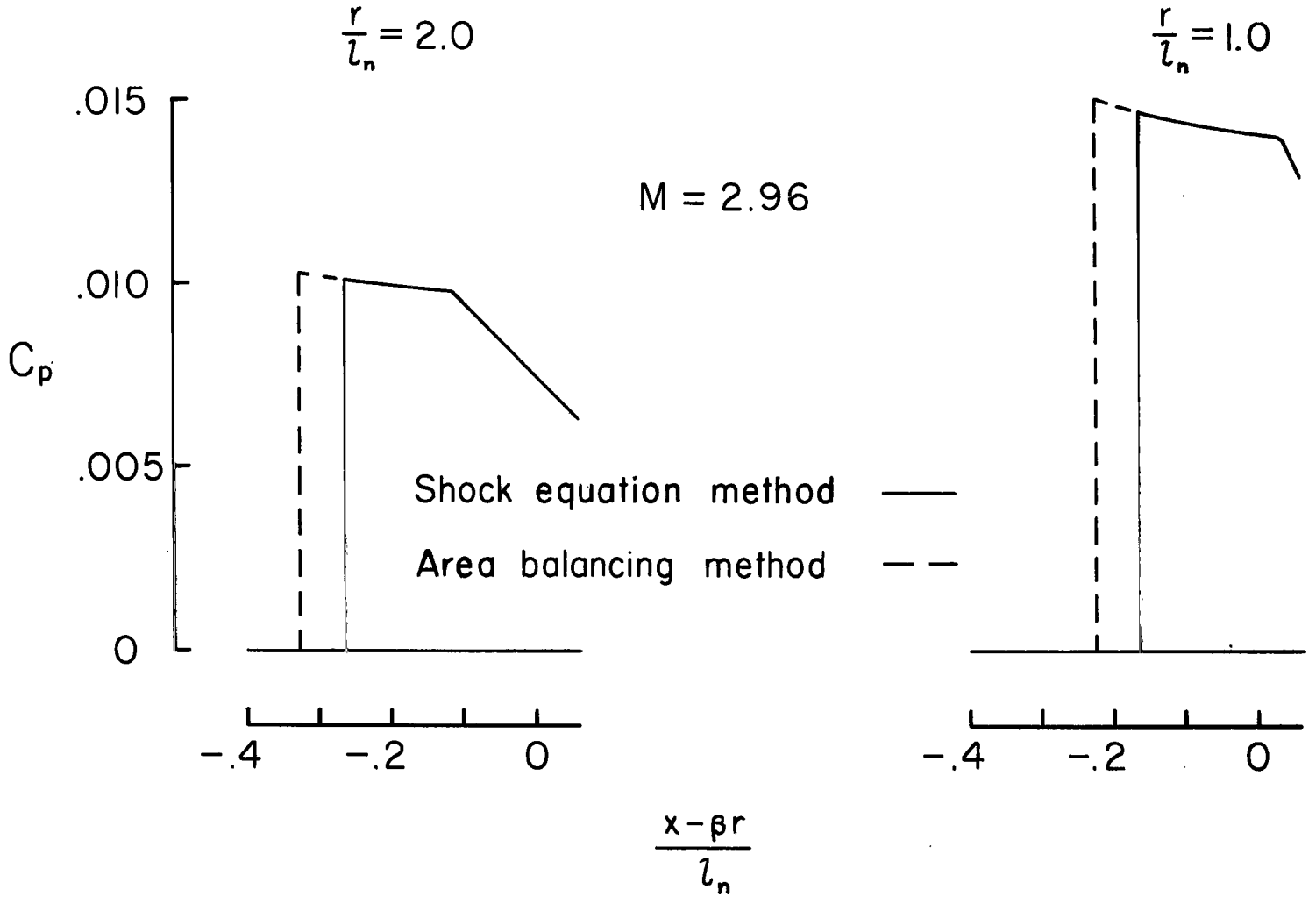

(d) Ducted-nacelle model.

Figure 9.- Concluded.

"The aeronautical and space activities of the United States shall be conducted so as to contribute . . . to the expansion of human knowledge of phenomena in the atmosphere and space. The Administration shall provide for the widest practicable and appropriate dissemination of information concerning its activities and the results thereof."

—NATIONAL AERONAUTICS AND SPACE ACT OF 1958

NASA SCIENTIFIC AND TECHNICAL PUBLICATIONS

TECHNICAL REPORTS: Scientific and technical information considered important, complete, and a lasting contribution to existing knowledge.

TECHNICAL NOTES: Information less broad in scope but nevertheless of importance as a contribution to existing knowledge.

TECHNICAL MEMORANDUMS: Information receiving limited distribution because of preliminary data, security classification, or other reasons.

CONTRACTOR REPORTS: Scientific and technical information generated under a NASA contract or grant and considered an important contribution to existing knowledge.

TECHNICAL TRANSLATIONS: Information published in a foreign language considered to merit NASA distribution in English.

SPECIAL PUBLICATIONS: Information derived from or of value to NASA activities. Publications include conference proceedings, monographs, data compilations, handbooks, sourcebooks, and special bibliographies.

TECHNOLOGY UTILIZATION PUBLICATIONS: Information on technology used by NASA that may be of particular interest in commercial and other non-aerospace applications. Publications include Tech Briefs, Technology Utilization Reports and Technology Surveys.

Details on the availability of these publications may be obtained from:

SCIENTIFIC AND TECHNICAL INFORMATION OFFICE

NATIONAL AERONAUTICS AND SPACE ADMINISTRATION

Washington, D.C. 20546